3

How Cyclones Work

As mentioned in Chap. 1, cyclones work as a result of the centrifugal forces acting on the particles suspended in the swirling gas stream. This causes the particles, which are denser than the gas, to move outward to the cyclone wall, along which they are transported downward to the dust exit. The cleaned gas leaves near the centerline, in a reverse-flow cyclone through the roof. In a 'once-through' or 'flow-through' cyclone, the cleaned gas exits out the bottom[1].

In this chapter we take a first look at the flow of gas and particles in cyclones. We also introduce the two key performance indicators for cyclones: their separation efficiency and their pressure drop.

3.1 Flow in Cyclones

The gas flow pattern in cyclones is fairly well known from experimental evidence collected over decades. For particle trajectories, on the other hand, very little experimental data are available, so for this we shall resort to computational fluid dynamics (CFD) simulations.

3.1.1 Gas Flow Pattern

The velocity field in cyclones has been measured using hot-wire anemometers, pitot tubes and, recently, laser-Doppler anemometry (LDA). See Chap. 10 for more information about these techniques.

[1] In some configurations, cyclones may be oriented at an angle to true vertical and, in the limit, may be oriented horizontally. Such configurations do not violate the rules and equations governing vertical cyclones except in certain 'highly loaded' cyclones, wherein the force of gravity competes with the radially-directed centrifugal force, which the particles experience. In such latter configurations the designer must be especially careful in scaling-up. We shall return to this topic in a later chapter.

Figure 3.1.1 shows a sketch of a standard reverse-flow cylinder-on-cone gas cyclone with a tangential entry. The global flow pattern is indicated. A swirling motion is created in the separation space by the tangential injection of the gas. The gas flows downward in the outer part of the swirl (the 'outer vortex') and upward in the center (the 'inner vortex'). The downward flow in the outer part of the cyclone is critically important as it, and not gravity, is the dominant mechanism for transporting collected solids (those at the wall) out the bottom of the cyclone. In vertically oriented cyclones, gravity will assist but its influence is important only for cyclones operating at high solids-loaded conditions, for which 'mass loading' effects are important. More on this later. At the same time there is a radial flow from the outer vortex to the inner one, this is distributed—though not uniformly with height—over the length of the body under the vortex finder.

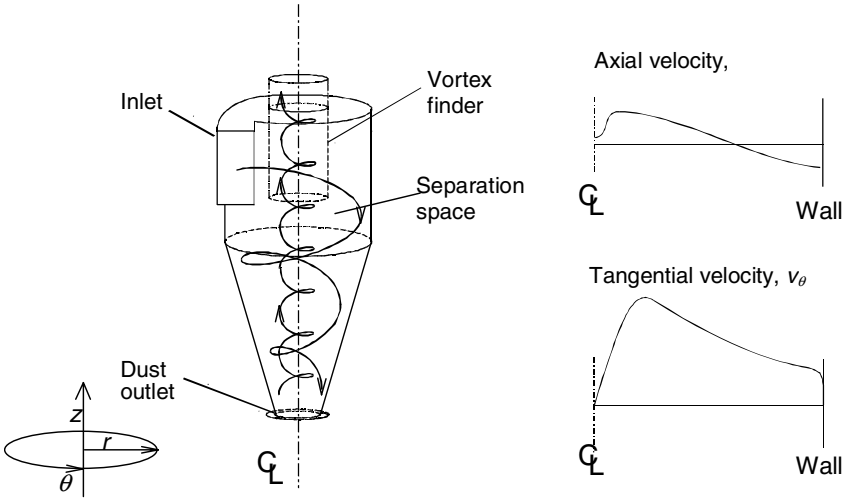

Fig. 3.1.1. Sketch of a tangential-inlet cyclone with the flow pattern indicated. The coordinate directions are shown, normally the z-axis coincides with the axis of the cyclone or swirl tube. To the right, the radial distributions of the axial and tangential gas velocity components are sketched. It is understood that the 'dust outlet' may be the 'liquid' outlet for the case of a demisting cyclone

To the right in Fig. 3.1.1 the radial profiles of the axial and tangential gas velocity components are sketched. The former shows the outer region of downwardly directed axial flow and the inner one of upwardly directed flow. As mentioned, the downward velocity at the wall is the primary mechanism for particle transport out the dust outlet. The axial velocity often shows a dip around the center line. Sometimes this is so severe that the flow there is downwardly directed. The tangential velocity profile resembles a Rankine vortex: a near loss-free swirl surrounding a core of near solid-body rotation.

We do not know enough about the radial velocity to graph it. It is generally much smaller than the tangential velocity and more difficult to measure accurately. It is generally inwardly directed below the lip of the vortex tube, but it is not uniform with height. Rather, the greatest inward flow occurs immediately below the vortex tube opening – this is related to the secondary flows discussed below.

As the discussion in Sect. 2.1.1, and Eq. (2.A.12) show, in order for a rotating fluid element to maintain its equilibrium (static position in the r-direction), the pressure on its surface at higher r must exceed that on its surface a lower r. Thus the static pressure must increase monotonically with increasing radius. This, in fact, is borne out by experiment—a classic example of which is the data of Ter Linden (1953), a sample of which is presented in Fig. 3.1.2. Here the lower curves contained within each set of curves represents the variation in static pressure, p, with radial position; the upper curves, the total pressure, $p+(1/2)\rho v^2$ (static plus dynamic). Comparing with Eq. (2.1.3) and realizing, as before, that the second term in Bernoulli's trinomial is small, we see from the profiles of total pressure in Fig. 3.1.2 that Bernoulli's trinomial is almost constant in the outer, nearly loss-free part of the vortex, while it decreases significantly in the center. This is as we would have expected.

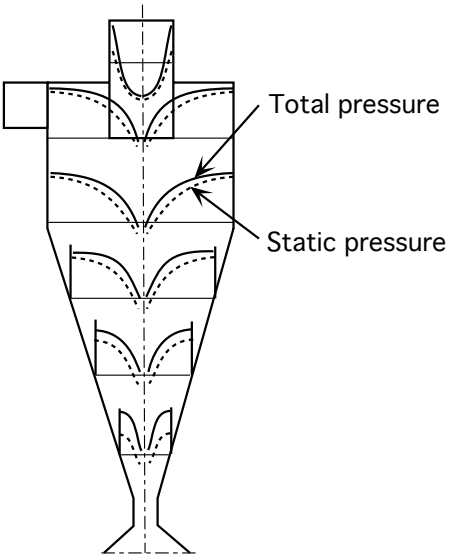

Fig. 3.1.2. Static and dynamic pressure profiles within a cyclone

These data also show that the static pressure within the vortex finder also increases with radial position. This is also what we would expect, since there is still swirl present there. In this "core" region the velocity is approximately that of solid-body rotation, i.e. Eq. (2.1.1). Additionally, the static pressure is

observed to be strongly dependent upon radial position and, like that within the main body of the cyclone, has its maximum value at the wall. Clearly, a simple static pressure measuring tap mounted flush with the inner wall of the vortex finder is not representative of the *average* pressure within this tube. We will have more to say about this in Sect. 4.1.2.

Swirl flow near the walls of concave surfaces is inherently unstable. Pressure gradients caused by the swirling motion create 'secondary flows' in the cyclone body along the walls. We saw in Chap. 2 that the static pressure increases toward the outer part of a swirling flow. This pressure gradient continues to persist through the boundary layers at the roof and at the conical wall. The tangential velocity, on the other hand, is low in these boundary layers. The result is a net inwardly directed force acting on gas pockets in the near-wall region, causing inwardly directed flows along the cyclone roof and the conical wall as indicated in Fig. 3.1.3, so that this net inward force is balanced by frictional drag with the wall and the bulk flow.

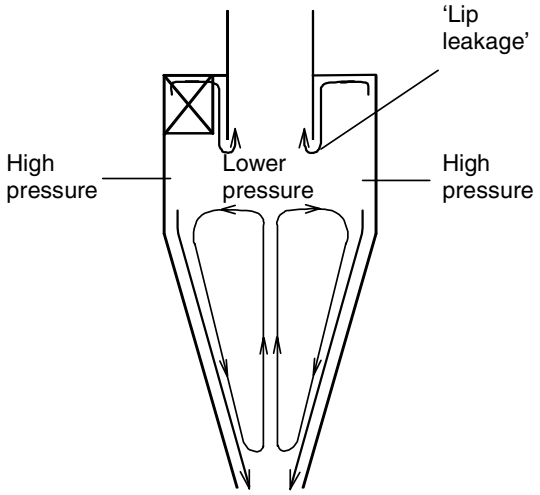

Fig. 3.1.3. The secondary flows caused by the swirl in the cyclone

The strong pressure gradient also has other effects, aside from the secondary flow patterns just mentioned, which are important for the flow near the wall within cyclones and within other such centrifugal devices including swirl tubes and hydrocyclones. In particular, let us apply the above concepts to the region of the boundary layer at the cyclone wall. Here we find that none of the velocity profiles we have discussed thus far apply since none of them predict a sharp decrease in v_θ within this "near wall" region as $r \to R$, where R is the cyclone radius at any given axial position. Nor do they account for the fact that $v_\theta = 0$ at $r = R$. In this wall region, as $v_\theta \to 0$, the 'cen-

trifugal force' that the fluid experiences becomes vanishingly small, and the static pressure experiences a negligible increase with radius. See Eq. (2.A.12), for example, which predicts $dp/dr \to 0$ for $v_\theta \to 0$. Consequently, *wall disturbances can cause the affected portion of the high pressure, solids-laden fluid near the wall to be deflected radially inward. In so doing the fluid will carry some of the previously collected solids with it, thereby degrading separation performance.* In a figurative sense, it is as though the high-pressure fluid near the wall is "just looking for an excuse" to break away from the wall and flow into the low-pressure inner regions of the cyclone. Flow over any concave surface is inherently unstable. This, then, is one reason why cyclone walls should be constructed and maintained as smooth as possible—free of any features which can disturb the flow. This includes such things as: weld seams, warped or distorted walls, solid deposits, damaged refractory or ceramic lining, eroded walls, sight-glasses, thermowells, light-ports, 'manways' or access ports/hatches (that are not flush and contoured to the inside surface of the cyclone), pressure sensors, areas that are hardfaced or 'weld overlaid', flange joints, gaskets that protrude into the flow, and most any area that has been previously repaired that is not in smooth 'like new' condition. This may even include walls that are out-of-round or walls fabricated from plate metal that have been crudely 'braked' and not 'rolled' to render smooth internal surfaces. Such nonideal conditions are virtually impossible to accurately simulate with existing models. Our models can handle uniform wall roughness, once this roughness is known. However, they cannot handle the nonideal wall conditions listed above. Yet, these conditions can strongly impair separation performance. For this reason, plant engineers, maintenance personnel, and designers need to be especially attuned to wall conditions and, should flow disturbances be found, take whatever steps are necessary and practical to render the walls smooth and free from such disturbances.

The secondary flows mentioned above drive others, in turn. For instance, the flow along the roof drives a downward flow along the outer wall of the vortex finder. This contributes to the high radial velocity just under the vortex finder wall, mentioned above, generally referred to as 'lip leakage'.

In addition to these secondary boundary layer flows, there is experimental evidence that a 'swiss roll' type of secondary flow pattern exists in the core of the cyclone body, as indicated in Fig. 3.1.3. Such a flow pattern can cause particles to recirculate in the cyclone body.

In general, many of the features of the flow in cyclones can be understood when considering the effects of the swirling motion on the axial and radial flow pattern. This issue will be discussed in Chap. 4.

3.1.2 Particle Flow

Particles entering the separation space are subject to an inwardly directed drag and an outwardly directed centrifugal force. The 'separation space' starts at the point, where the incoming gas first experiences rotational flow and

the particles carried along in this gas flow first experience a centrifugal force acting radially outwards. This point varies with inlet design and may start, for example, at the leading edge of an inlet scroll or helix upstream of the upper 'barrel' section of the cyclone proper.

Irrespectively, the centrifugal force is proportional to the particle mass and, therefore, the cube of the particle diameter: x^3. The drag force, which is due to the flow of gas from the outer to the inner part of the vortex, is proportional to x, at least when Stokes' law applies which it often does in practice. The largest particles are therefore the easiest to separate.

It is not easy to study the particle flow pattern experimentally. In order to give an impression of the flow of a particle through a cyclone, we can resort to CFD simulations. Figure 3.1.4 shows a series of particle trajectories. The particles are injected at different radial positions along the inlet in a precalculated gas flow field. The swirling motion is not shown.

Although the object is to centrifuge the particles to the wall and capture them, it is interesting to look at particles so fine that some of them are not collected. An extremely fine 1.0 μm particle size was used to generate the particle paths shown in Fig. 3.1.4. Some of the particles can be seen to exit through the vortex finder, while those injected closer to the wall, reach the wall, where they are deemed to be captured and are removed from the simulation.

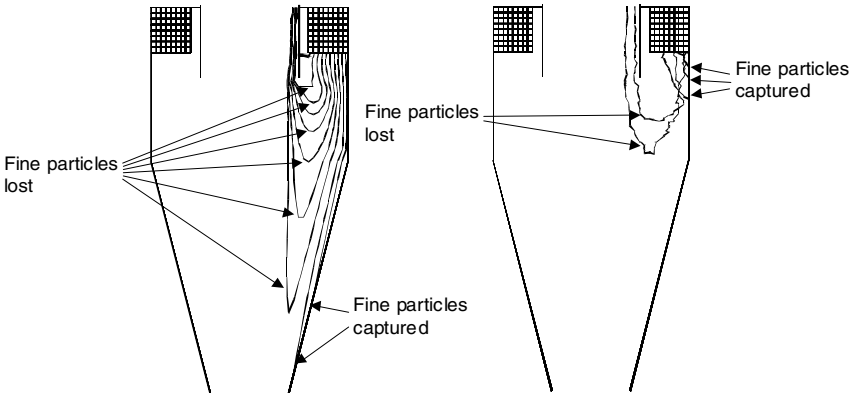

Fig. 3.1.4. Particle tracks in a cyclone by computational fluid dynamics. The swirl components are not shown. On the left 10 tracks are calculated from the mean flow field; on the right 5 particle tracks are shown where the response to the turbulent motion of the gas is taken into account. Conditions: cyclone diameter: 20 cm, gas inlet velocity: 15 m/s, gas at SATP ('standard ambient temperature and pressure', 25°C and 1 atm), particle density: 2730 kg/m^3

3.2 Separation Efficiency

3.2.1 Overall Separation Efficiency

The three particle fractions we are concerned with in cyclone operation are the *feed*, the *captured* (or collected or 'underflow') and the '*overflow*' (or emitted or lost) fractions. Let us represent their masses (or mass flow rates) by the symbols M_f, M_c and M_e, respectively. The mass balance for solids over the cyclone is:

$$M_f = M_c + M_e. \tag{3.2.1}$$

The overall separation efficiency η is simply calculated as the mass fraction of the feed solids captured by the cyclone:

$$\eta = \frac{M_c}{M_f} = 1 - \frac{M_e}{M_f} = \frac{M_c}{M_c + M_e}. \tag{3.2.2}$$

The efficiency is determined by collecting samples and weighing two of the fractions.

The overall efficiency is usually what counts the most in the context of an industrial process. However, it is not a good measure for characterizing the intrinsic separation performance of a particular cyclone, since, for example, it tells us nothing about the separation capability of the cyclone as a function of particle size.

3.2.2 Grade-Efficiency

The separation characteristics of a cyclone are best described by the so-called grade-efficiency curve or GEC, which is the separation efficiency for a given feed particle size or (narrow) range of particle sizes.

If the differential volume or mass density distributions of the charge dust, the captured and overflow (or emitted) fractions are $f_f(x)$, $f_c(x)$ and $f_e(x)$, respectively, the mass balance for particles with diameter between $x - 1/2\ dx$ and $x + 1/2\ dx$ is:

$$\begin{aligned} f_f\,(x)\,dx = \eta f_c\,(x)\,dx + (1-\eta)\,f_e\,(x)\,dx = dF_f\,(x) \\ = \eta dF_c\,(x) + (1-\eta)\,dF_e\,(x)\,. \end{aligned} \tag{3.2.3}$$

To help make this a little less abstract, let us approximate the particle size differential with a finite, yet small value for dx, and also substitute in some numbers obtained from a hypothetical cyclone performance measurement: Thus, let us assume we determine (through measurements) that 10% of the feed solids (by wt. or vol.) lie within a 5-micron (Δx) band centered about some particular particle size, x. In addition, the measurements show that 80% of the particles within this particular 5-micron band are collected and that they comprise 6% of the collected material. Likewise, 30% of the

particles are emitted ("lost") and they comprise 26% of the emitted solids. Our finite approximation to the left three terms of Eq. (3.2.3) then reads:

$$0.10 \times 5 = 0.08 \times 0.06 \times 5 + (1 - 0.80) \times 0.26 \times 5$$

or, cancelling the Δx's (i.e. the 5's):

$$0.10 = 0.048 + 0.052 = 0.10$$

Thus, we see that the cyclone brings about the mathematical equivalent of a partition function, η—it partitions the particles in any given size range, Δx, into the underflow and overflow streams. It does this on the basis of the forces acting on the particles within the separation zone of the cyclone.

Equation (3.2.3) can be integrated term-by-term to give a mass balance for the dust with particle size less than a given size x:

$$F_f(x) = \eta F_c(x) + (1 - \eta) F_e(x) \tag{3.2.4}$$

The grade-efficiency is defined as the fraction of the feed solids with diameter between $x - 1/2\ dx$ and $x + 1/2\ dx$ that is captured in the cyclone:

$$\eta(x) = \frac{M_c f_c(x)\, dx}{M_f f_f(x)\, dx} \tag{3.2.5}$$

Making use of Eq. (3.2.2) and of the mass balances in Eqs. (3.2.3) and (3.2.4) gives:

$$\eta(x) = \eta \frac{f_c(x)}{f_f(x)} = 1 - (1 - \eta) \frac{f_e(x)}{f_f(x)} = 1 - (1 - \eta) \frac{dF_e(x)}{dF_f(x)} \tag{3.2.6}$$

A typical grade-efficiency curve is sketched in Fig. 3.2.1.

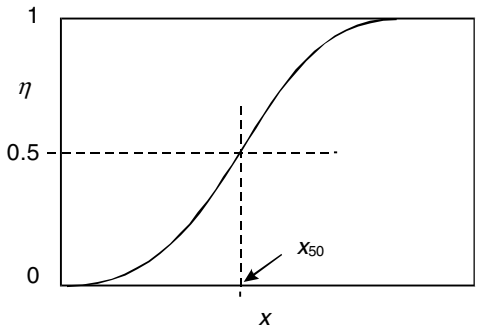

Fig. 3.2.1. Sketch of a typical, s-shaped grade-efficiency curve

If the separation in the cyclone was ideally sharp, the grade-efficiency curve would be a vertical line at the 'critical' or 'cut' size, x_{50}. For a number of reasons—two of which we have considered already—this is not so:

- particles of the same size may be either captured or lost depending on their entry position in the inlet,
- turbulent particle dispersion due to normal fluid turbulence, and enhanced by such things as internal wall roughness and surface irregularities, leads to backmixing,
- particles greater than x_{50}, which were already separated, may be reentrained low in the cyclone or in the dust hopper if the cyclone's lower section is not carefully designed,
- particles smaller than x_{50} may agglomerate with larger ones, and be separated
- particle attrition may take place within the cyclone.

For these reasons we obtain a smooth, s-shaped, grade-efficiency curve in practice. The *cut size*, or 'x-50 cut-point' (often referred to as the 'd-50 cut-point diameter') is taken as the size that is separated with a fractional efficiency of 0.5: x_{50}.

Unlike gross or overall efficiency, a cyclone's x-50 cut-point and grade-efficiency curve are true measures of its intrinsic separation potential. These properties are independent of the size distribution of the feed, at least under low solids loading conditions. We shall return to this issue later.

The x_{50} size is exactly analogous to the openings in an ordinary screen or sieve. In a sieving operation, all feed particles greater than x_{50} will be captured or 'retained', and all less than x_{50} will not be captured. In practice, even a sieve exhibits some nonideal separation with respect to particle size but, generally speaking, a sieve very closely approximates a perfectly sharp separator: it tends to retain all particles greater than its x-50 cut-size or cut-point (sieve opening) while losing those less than its cut-point. In practice, it is often useful to think of a cyclone as a 'sieve', especially when it performs a particle classification duty as opposed to a bulk solids separation task. More on this later.

Furthermore, if the grade-efficiency is reported in terms of an aerodynamic particle size (see Sect. 2.3.1) by calculating this from the actual particle sizes, it is also independent of the density of the feed particles and truly a characteristic of the cyclone. The aerodynamic particle size can be calculated from the actual particle sizes.

The steepness of the grade-efficiency curve around the cut size is an indication of the 'sharpness of the cut' of the cyclone. One measure for this is simply the gradient of the grade-efficiency curve at x_{50}, another is the ratio of the diameters corresponding to two specific fractional efficiencies, for instance 0.25 and 0.75: x_{25}/x_{75}.

The measures of sharpness reported above are two ways of representing the true slope of the grade-efficiency curve near its cut-point, $x_{50.}$ However, in many applications one can mathematically fit the cyclone's measured grade-efficiency data to some functional form $\eta = f(x_i)$ and, with appropriate transformation of the variables, plot the data so that it appears as a straight - or

nearly straight - line. Such a line will also have a 'slope' but this slope will be constant over the entire range of particle sizes and different than the 'true' grade-efficiency curve slope described in the previous paragraph. Nevertheless, both slopes are useful and we will encounter this latter type of slope in Chaps. 5 and 6.

3.2.3 Converting Between Overall Efficiency and Cut-size

We often have occasion to convert between the overall efficiency η and the cut size x_{50}, for instance, when we wish to compare an efficiency determined by testing with the cut-size predicted by a model. There are two ways of doing this: a simple approximation and the precise way.

The simple approximation is to assume the cyclone to have a sharp cut at x_{50}, *i.e.* that all material below x_{50} is lost and all material above is collected. If the cumulative undersize distribution of the feed is $F_f(x)$, then (see Fig. 3.2.2):

$$1 - \eta = F_f\left(x_{50}\right) \tag{3.2.7}$$

The precise way is to use the entire grade-efficiency curve for the cyclone, $\eta(x)$. The fraction of feed lying within the band $x - 1/2\ dx$ and $x + 1/2\ dx$, is captured with a fractional efficiency of $\eta(x) f_f(x) dx$. The total fraction of the feed captured is therefore:

$$\eta = \int_0^\infty \eta\left(x\right) f_f\left(x\right) dx = \int_0^\infty \eta\left(x\right) dF_f\left(x\right). \tag{3.2.8}$$

Experience shows that the approximate method (Eq. 3.2.7) comes out surprisingly accurate, even when the cut of the cyclone is far from sharp. This has very practical implications and is often used when one just needs a rough estimate of overall separation efficiency.

3.3 Pressure Drop

We finally look briefly at cyclone pressure drop. The normal procedure for measuring a pressure drop in the process industry is to measure the static pressure at the wall in the upstream and downstream piping or ducting. This is complicated in cyclones by the swirl in the exiting gas. In the first place, the swirl causes the static pressure at the wall to be higher than the cross-sectional average, and in the second place, there is the issue of what to do with the dynamic pressure stored in the swirling motion. We shall consider the options for solving these problems in Chap. 4. Here it suffices to say that when we talk of the 'pressure drop' over the separator, we mean the drop in *total* pressure: the sum of the static and dynamic pressures.

The pressure drop over a cyclone is normally subdivided in three contributions:

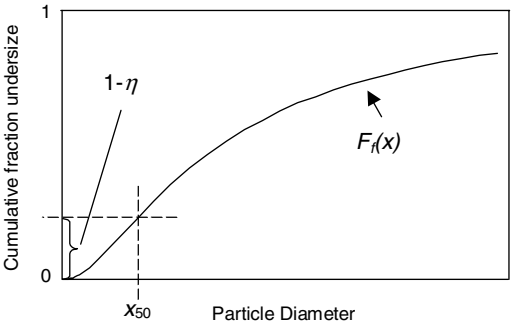

Fig. 3.2.2. Sketch showing the principle of determining the overall efficiency from the cumulative size distribution of the feed and the cut size

1. losses in the entry,
2. losses in the separation space (the main cyclone body), and
3. losses in the vortex finder.

The losses in the entry are often negligible compared to the other contributions, at least in tangential entry cyclones. For swirl tubes with inlet vanes little information is available, but if the vanes are properly contoured aerodynamically, the losses are generally small.

The losses in the cyclone body are higher, but, as we shall see later, their main significance is in limiting the intensity of the swirl in the separation space: more frictional losses at the walls lead to a less intensive vortex. Such *wall losses* do not dominate the overall pressure drop.

The losses in the vortex finder are the largest, in both through-flow and reverse-flow tangential-inlet cyclones. Vortex finder losses may be an order of magnitude larger than the two other contributions. The one notable exception is highly (solids) loaded primary or 'rough-cut' cyclones wherein wall losses associated with frictional drag at the walls can become a significant contribution to the overall pressure loss—at the expense of losses in the vortex core, and the vortex finder.

The pressure drop over a cyclone, Δp, is proportional to—or very close to being proportional to—the square of the volumetric flowrate, as it is in all processing equipment with turbulent flow. To obtain a characteristic measure for pressure drop in a given cyclone, pressure drop is often reported in a dimensionless form known as the 'Euler number':

$$Eu \equiv \frac{\Delta p}{\frac{1}{2}\rho\langle v_z\rangle^2} \tag{3.3.1}$$

where $\langle v_z\rangle$ is the mean axial velocity in the cyclone body, *i.e.* the volumetric flow rate divided by the cross-sectional area of the cylindrical part of the body.

It does not matter which velocity we use to define the Euler number. While the definition in (3.3.1) is popular in research laboratories, most practicing

engineers prefer to use either the inlet velocity or the mean velocity in the vortex finder, since these are the velocities most commonly reported by vendors and designers as part of their overall performance summary:

$$Eu_{in} \equiv \frac{\Delta p}{\frac{1}{2}\rho v_{in}^2}; \qquad Eu_x \equiv \frac{\Delta p}{\frac{1}{2}\rho v_x^2}. \tag{3.3.2}$$

Equation (3.3.2) is especially useful to the plant engineer who wishes to estimate the pressure loss through his or her cyclone system at conditions other than design conditions, or at some flow rate other than one for which the pressure loss is known. We shall see how in Chap. 8, where also the derivation of this and other dimensionless numbers characterizing cyclones and swirl tubes can be found.

With this discussion, we have introduced the basic working characteristics of gas cyclones. In Chaps. 4, 5 and 6 we shall consider the gas flow pattern and the separation in more detail, and also models for predicting them as reported in the research literature. In Chap. 10 we will discuss how cyclone performance can best be determined from laboratory and/or plant measurements.

3.A Worked Example: Calculating a Grade-Efficiency Curve

Let us say that we have measurements of the cumulative undersize distributions for the feed and the lost fractions. The overall fractional efficiency has been measured to be η=0.88. We wish to calculate the grade-efficiency curve.

The cumulative size distributions are:

Feed:

x_i (μm)	1.5	2.5	3.75	5.25	7.0	8.5	9.6	11.4	13.1	14.8	16.8	18.5
$F_f(x_i)$	0	0.01	0.09	0.22	0.37	0.57	0.68	0.78	0.87	0.94	0.98	1.0

Overhead fraction:

x_i (μm)	1.75	2.4	2.9	3.25	3.5	4.0	4.6	5.5	6.5	7.3
$F_e(x_i)$	0.047	0.10	0.30	0.45	0.54	0.70	0.83	0.94	0.99	1.0

Solution

The equation we need to use is Eq. (3.2.6). One option we might consider is to fit model distribution functions, such as the ones we looked at in the

previous chapter, to the data and then using Eq. (3.2.6) directly to determine grade-efficiency performance. However, this will usually not work unless the data are fitted extremely well in the fine end. The small discrepancies between data and fitted function for the smaller size particles of the distributions will otherwise lead to totally wrong grade-efficiency data.

We therefore use the discrete equivalent of Eq. (3.2.6) on the data as they are and calculate, using a spreadsheet for example, the separation efficiency in a series of size intervals, as follows.

The discrete equivalent of Eq. (3.2.6) is:

$$\eta\left(\frac{x_i + x_{i+1}}{2}\right) = 1 - (1-\eta)\,\frac{(F_e\,(x_{i+1}) - F_e\,(x_i))}{(F_f\,(x_{i+1}) - F_f\,(x_i))} \tag{3.A.1}$$

In order to use this equation, we need data for F_e and F_f at the same x_i. We interpolate the function F_f to the points at which we have F_e. Linear interpolation gives:

Feed interpolated:

x_i (μm)	1.75	2.4	2.9	3.25	3.5	4.0	4.6	5.5	6.5	7.3
$F_f(x_i)$	0.0025	0.009	0.036	0.058	0.074	0.112	0.164	0.241	0.327	0.410

Filling in values for the first interval in (3.A.1):

$$\eta\,(2.08) = 1 - (1 - 0.88)\,\frac{(0.10 - 0.047)}{(0.009 - 0.0025)} = 0.022$$

The result of doing this for all the intervals are the points on the grade-efficiency curve shown in Fig. 3.A.1. This completes our solution to the problem.

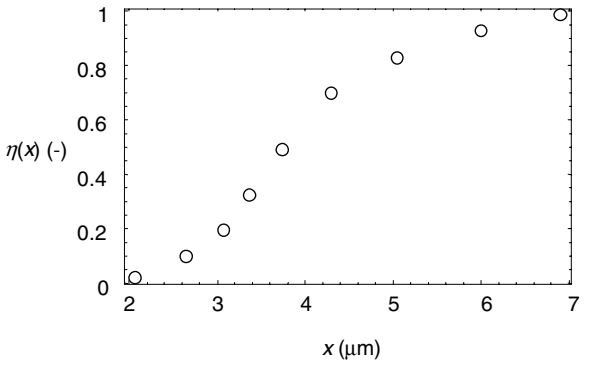

Fig. 3.A.1. Grade-efficiency data calculated from Eq. (3.A.1)

It only takes a small change in the F-data to generate quite different grade-efficiency points, particularly at small x_i. A high quality of size analyses is therefore necessary for generating reliable grade-efficiency curves, especially for the finer particle sizes. Even changing the interpolation from linear to one of higher order changes the first two points. In practice, linear interpolation often works the best, being the least sensitive to small errors in the experimental points.

Generation of accurate grade-efficiency curves is often left to sampling and measurement specialists who are very familiar with the technology under examination and with all the factors that can give rise to erroneous results if they are not adequately accounted for. These include, but are not limited to:

1. Solids maldistribution in the ducts being sampled.
2. Inability to obtain a reasonable match between the velocity entering the sampling probe and that within the duct being measured (*i.e.* inability to achieve 'isokinetic sampling').
3. Flow conditions in which isokinetic sampling is difficult or impossible, such as a skewed velocity profile or strong swirl flow.
4. Insufficient sample mass.
5. Vapor condensation as solids are being withdrawn.
6. Solids agglomeration or dispersion upon measurement of their particle size (after sample is caught).
7. Unsteady gas and/or solids flow conditions during sampling
8. Solids 'reacting' or otherwise being transformed upon sampling into a size distribution other than that which exist in the operating unit.
9. Human error.

Most of these issues will be discussed in Chap. 10.